Journal of Sustainable Development of Energy, Water and Environment Systems

http://www.sdewes.org/jsdewes

Year 2026, Volume 14, Issue 4, 1140750

Original Research Article

Integrated Pinch–Life Cycle Assessment Framework for Energy and Environmental Optimization of Industrial Processes toward Carbon Neutrality

Jesunino R. Aquino*[1,2], Bonifacio T. Doma[2], Maribel G. Songsong[1,2]
Jian Carlo M. Guevara[1], Ariane Ysabel M. Mitra[1], and James Christian T. Pacia[1]

[1]College of Engineering, Mapua Malayan Colleges Laguna, Cabuyao, Laguna, 4025, Philippines
e-mail: jraquino@mcl.edu.ph; mgsongsong@mcl.edu.ph; 2023jcmguevara@live.mcl.edu.ph; 2023aymmitra@live.mcl.edu.ph; 2023jctpacia@live.mcl.edu.ph.;
[2]School of Graduate Studies, Mapua University, Intramuros, Manila, 1002, Philippines
e-mail: btdoma@mapua.edu.ph

Cite as: Aquino, J. R., Doma, B. T., Songsong, M. G., Guevara, J. C. M., Mitra, A. Y. M., Pacia, J. C. T., Integrated Pinch–Life Cycle Assessment Framework for Energy and Environmental Optimization of Industrial Processes toward Carbon Neutrality, J.sustain. dev. energy water environ. syst., 14(4), 1140750, 2026, DOI: https://doi.org/10.13044/j.sdewes.d14.0750

ABSTRACT

This study presents an integrated framework combining thermal pinch analysis and life cycle assessment to evaluate energy-intensive industrial processes, addressing the need to capture both operational efficiency and environmental impacts. The goal is to determine whether energy savings from process integration justify associated environmental burdens. The method links utility targets and heat exchanger network designs with life cycle inventory data, while explicitly including heat exchanger manufacturing impacts. Three industrial cases—ammonia, bioethanol, and hydrogen production from biomass-based resources—were analyzed. Results show energy use reductions of 62.27–76.05% and cost savings of 45.81–65.38%. Environmental impacts, including global warming and resource depletion, decreased significantly, although minor trade-offs appeared in ozone depletion and mineral resource use due to added equipment. The framework reveals hidden burden shifting and supports transparent decision-making for industrial decarbonization strategies.

KEYWORDS

Process integration, Thermal pinch analysis, Life cycle assessment, Carbon neutrality, Energy optimisation, Environmental optimisation, Sustainable industrial systems.

INTRODUCTION

The industrial sector remains one of the largest consumers of energy worldwide and a major contributor to greenhouse-gas emissions, making industrial decarbonisation a central challenge in the transition toward carbon neutrality [1]. In energy-intensive industries, heating, cooling, compression, and utility generation are closely linked to fossil fuel consumption, air emissions, and fluctuating energy demand [2]. These systems are further complicated by interactions among water, energy, materials, and pollution-control requirements, which require decision

* Corresponding author

tools that can evaluate efficiency, retrofit feasibility, and environmental consequences simultaneously [3].

Recent process-integration studies confirm that thermal pinch analysis remains a practical first-principles method for reducing external heating and cooling demand in industrial systems. Comendador et al. demonstrated that heat integration can remove external heating requirements in a biomass fast-pyrolysis and sorption-enhanced steam-reforming process [4]. Wang et al. combined heat integration with thermodynamic, environmental, and economic evaluation for biomass gasification and reported substantial performance improvements [5]. Alqahtani et al. showed that pinch-based heat and power integration can reduce energy expenses in chlorobenzene production with only a moderate capital increase [6]. Corrêa et al. embedded heat integration in rigorous optimisation models that account for multiple utilities and thermodynamic properties [7]. Gu et al. extended the concept to interplant heat-exchanger-network opportunities in industrial parks [8]. Lipiainen et al. further showed that hydrogen transport choices affect cost, efficiency, and greenhouse-gas emissions in industrial settings [9]. Hassan et al. reviewed heat-transfer modelling in steelmaking converters, highlighting the importance of accurate thermal descriptions for high-temperature industrial systems [10]. Nutakki et al. integrated combined cooling, heating, power, and desalination concepts with biomass-fuelled energy systems, confirming the need to evaluate energy, economic, and environmental effects together [11].

Recent literature on biomass conversion and low-carbon fuels also supports the selection of the case studies used in this work. Pati et al. combined techno-economic, risk, and life cycle analysis for lignocellulosic biomass valorisation through co-gasification and syngas fermentation [12]. Ahuja et al. reviewed syngas fermentation to bio-alcohols and identified conversion, tolerance, and scale-up challenges [13]. Safarian et al. modelled bioethanol production through herbaceous and agricultural biomass gasification integrated with syngas fermentation [14]. Phan et al. optimised hydrogen production from biogas using process simulation, thereby providing a representative gas-processing basis for evaluating thermal integration and environmental performance [15].

In parallel, life cycle assessment has become the dominant methodology for evaluating environmental burdens that extend beyond direct on-site energy consumption. Kleinekorte et al. highlighted the importance of embedding life cycle assessment directly into chemical process, product, and supply-chain design to avoid burden shifting across system stages [16]. Bjørn et al. emphasized that absolute environmental sustainability assessment requires evaluation of multiple impact categories rather than reliance on single indicators [17]. Bogacka et al. showed that life cycle assessment of metallurgical process-gas utilisation can reveal environmental trade-offs that are not apparent from energy analysis alone [18]. Koch et al. demonstrated that the choice of life cycle impact assessment method can materially affect conclusions in process-development assessment [19]. Fabris et al. showed that refrigeration-related life-cycle emissions can significantly affect total environmental performance [20]. Rashedi and Khanam illustrated how midpoint and endpoint indicators may lead to different interpretations of renewable-energy technologies [21]. Boix Rodríguez et al. demonstrated that heat-exchanger eco-design requires equipment manufacture to be considered as part of environmental evaluation [22]. Huijbregts et al. provided the ReCiPe 2016 impact assessment method used to convert inventory flows into midpoint and endpoint indicators in this study [23].

Despite these advances, a clear methodological gap remains at the interface of thermal pinch analysis, life cycle assessment, and industrial decarbonisation. Many studies stop after reporting energy targets and total annual cost following pinch analysis, while other studies report environmental performance largely through carbon-dioxide-equivalent metrics alone. What remains less common is a retrofit-sensitive workflow in which utility targets, heat-exchanger-network structure, exchanger area, and exchanger-manufacturing mass are transferred explicitly into the life cycle inventory. The distinctive feature of the present study

is therefore not the simple sequential use of pinch analysis followed by life cycle assessment, but the explicit propagation of retrofit outputs from Aspen Energy Analyzer into the environmental inventory so that both operating savings and equipment-related burdens are evaluated together.

Accordingly, this study develops and demonstrates an integrated thermal pinch analysis–life cycle assessment workflow for screening industrial decarbonisation options in three representative process industries: ammonia production from biomass, bioethanol production from biomass, and hydrogen production from biogas. The working hypothesis is that thermal integration will substantially reduce external utility demand and associated environmental impacts, and that these reductions will remain dominant even after the embodied impacts of additional heat-exchanger manufacture are included. A second hypothesis is that the integrated workflow will reveal case-dependent trade-offs that cannot be identified from energy analysis alone. The specific scientific contributions are: (i) a reproducible transfer protocol from process simulation and pinch-analysis outputs to a retrofit-sensitive life cycle inventory; (ii) an explicit interpretation of exchanger area and exchanger-manufacturing mass as decision variables linking heat-exchanger-network synthesis and life cycle assessment; and (iii) case-based discussion of practical network issues such as stream splitting, loop formation, residual utility placement around the pinch, and the feasibility of very-high-temperature heat recovery. The remainder of the paper is organized as follows. The Methods section defines the integrated workflow, model assumptions, data constraints, and life cycle impact assessment procedure. The Results and Discussion section reports the thermal integration results and the environmental consequences of each retrofit. The Conclusions section interprets the broader implications for industrial decarbonisation and practical implementation.

METHODS

The objective of this study is to compare baseline and thermally integrated process configurations using a coupled TPA-LCA workflow. For each case study, a converged Aspen Plus simulation was first developed to generate stream temperatures, enthalpy flows, and utility demands. These streams were then transferred to Aspen Energy Analyzer (AEA) to determine the pinch temperature, heat recovery approach temperature (HRAT), heat-exchange network (HEN) configuration, utility targets, exchanger areas, and total annual cost. The resulting changes in utility demand and heat-exchanger requirement were subsequently translated into life cycle inventory flows, after which midpoint and endpoint environmental impacts were calculated. The integrated workflow therefore links process simulation, thermal integration, and environmental assessment in a single chain of calculations instead of treating them as isolated exercises.

Overall integrated workflow

Figure 1 should be read as a six-step workflow: (1) baseline process simulation and convergence in Aspen Plus; (2) extraction of hot and cold stream data from the converged baseline model; (3) thermal pinch analysis and HEN synthesis in Aspen Energy Analyzer using HRAT screening and total annual cost minimisation; (4) translation of the modified utility targets, exchanger area requirements, and exchanger-manufacturing mass estimates into life cycle inventory flows; (5) midpoint and endpoint impact calculation using ReCiPe 2016; and (6) comparative interpretation of baseline, stand-alone thermal integration results, and integrated TPA-LCA results. The integration claim of this paper lies in steps (3) to (5), where retrofit outputs are propagated into environmental accounting.

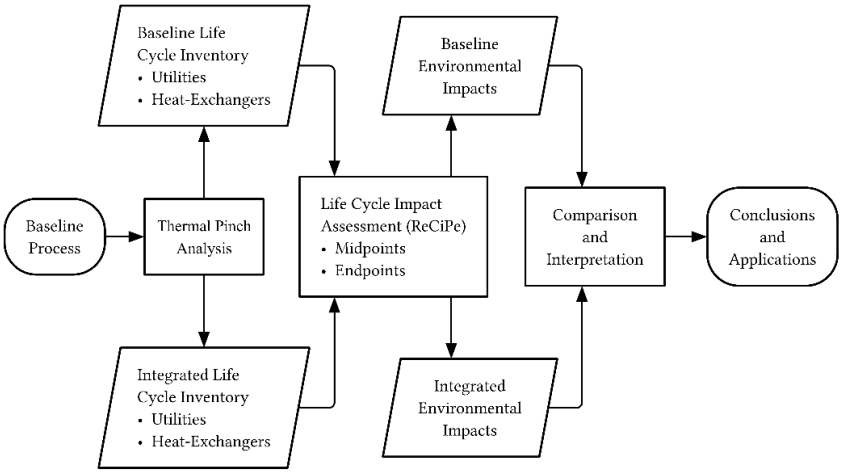

Figure 1. Pinch analysis and LCA framework.

Streamlined life cycle assessment

The LCA framework is comprised of four primary stages: the goal and scope definition, inventory analysis, impact assessment, and interpretation.

Goal and scope definition

This study focuses on life cycle phases that are affected by the application of energy integration. For this reason, the stages of cradle-to-gate were chosen, as shown in Figure 2. The figure shows that the foreground system is the chemical process, in which the design phase takes place, and the background system is the upstream processes of utility generation and heat-exchanger manufacturing. This deliberately focused cradle-to-gate scope does not represent a full product LCA; instead, it was selected to isolate the environmental consequences of HEN retrofit decisions. Raw material procurement, process effluents, product use, and end-of-life were not considered because they were assumed to remain unchanged between the baseline and integrated designs and would therefore not affect the comparative conclusions regarding pinch retrofit.

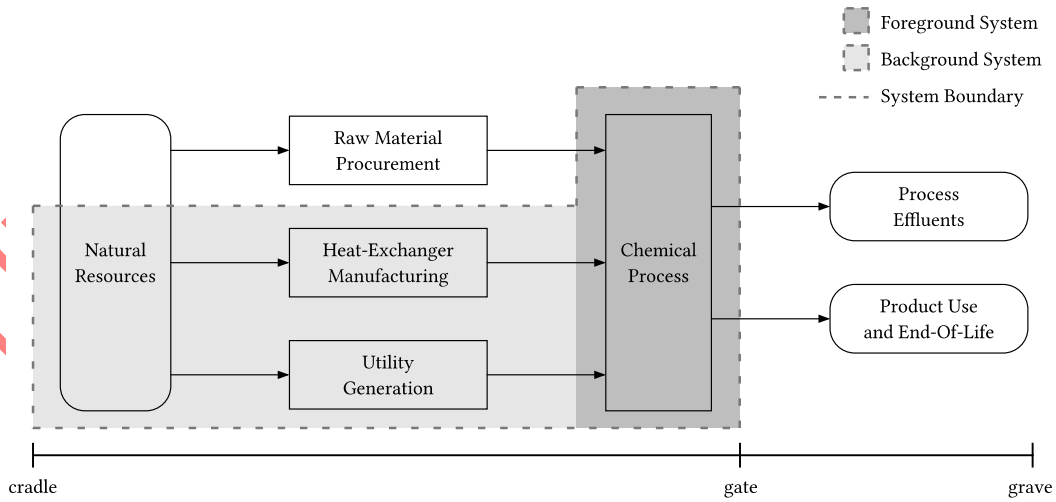

Figure 2. System boundary of the chemical processes in the life cycle assessment.

The selected midpoint indicators were GWI, SOD, POC, WU, MRD, and FRD because these categories could be supported consistently by the available retrofit-sensitive inventory data. The functional unit was defined as 1 kg of feed processed. Although this functional unit is process-centered rather than product-centered, it is appropriate for the present study because

the objective is to compare baseline and thermally integrated process configurations on an equivalent throughput basis and to isolate the environmental consequence of HEN design decisions.

Life cycle inventory assessment

The chemical processes of interest were modelled in Aspen Plus V14 to obtain mass and energy balances, stream temperatures, pressures, phase behavior, and utility duties. The converged models were then transferred to Aspen Energy Analyzer V14 for thermal pinch analysis and HEN synthesis. The property methods were selected according to the dominant phase behavior of each process. For the ammonia case, the Soave-Redlich-Kwong equation of state with Boston-Mathias alpha correction was used for conventional components, while HCOALGEN and DCOALIGT were used for nonconventional biomass and ash components. For the bioethanol case, Peng-Robinson with Boston-Mathias modification was used for conventional components, again with HCOALGEN and DCOALIGT for nonconventional solids. For the hydrogen case, the biogas-to-hydrogen system was modelled using an equation-of-state framework suitable for high-temperature gas processing, consistent with the source model by Phan et al. [15]. Reactor blocks were represented as RGIBBS, RSTOIC, REQUIL, flash, and separator units according to the level of reaction or separation detail available from literature sources.

Aspen Energy Analyzer provides preconfigured plant utilities such as fired heat, steam at several pressure levels, cooling water, cooling air, refrigeration, and hot oil. In this study, HRAT was screened using the software-generated trade-off curves for operating cost, capital cost, and total annual cost. The selected HRAT for each case corresponds to the minimum total annual cost reported by the software. While the optimisation engine is implemented internally by Aspen, its practical role in this work is to identify a near-optimal HEN through duty reallocation, stream splitting, and exchanger sizing subject to thermal feasibility constraints.

The life cycle inventory was defined by two groups of flows: operational utility consumption and equipment-related material demand. Operational flows included natural gas combustion, electricity for pumping and fanning, steam generation, refrigeration, cooling water, cooling air, and hot-oil circulation where relevant. Equipment-related burden was represented through exchanger area and an estimated exchanger-manufacturing mass derived from the area-shell correlation described later. Only data flows that were changed by thermal integration were propagated into the LCA model. This rule ensures that the integrated TPA-LCA comparison isolates retrofit-related differences instead of re-estimating the entire life cycle of the product systems.

Thermal pinch analysis and heat-exchange network synthesis

Thermal pinch analysis was carried out in Aspen Energy Analyzer V14 using the imported Aspen Plus stream data. For each process, the minimum hot utility, minimum cold utility, pinch temperature, and HRAT were obtained by composite-curve and cost-curve screening. The candidate HEN was then synthesized and refined by the software through stream splitting and duty allocation with total annual cost as the objective function. Although the internal optimisation routine of Aspen Energy Analyzer is proprietary, the decision variables directly affecting this study are the utility targets, exchanger duties, exchanger areas, and the number of shells required for the resulting network. These variables constitute the link between TPA and LCA. In the discussion of the resulting HENs, looped structures are interpreted as consequences of practical stream splitting and multi-match heat recovery rather than as thermodynamic violations per se; however, their presence signals increased control complexity and therefore they are discussed explicitly in the case-study sections.

For clarity, the baseline flowsheets shown in Figure 4, Figure 7, and Figure 10 model all process heating and cooling duties through utility heat exchangers. This baseline representation was intentionally adopted so that the retrofit opportunity identified by thermal pinch analysis

could be evaluated against a common reference. The integrated designs do not simply replace one utility exchanger at a time; rather, they reassign duties across matched hot and cold process streams, reduce external utility purchase, and alter exchanger area and network complexity. Consequently, the reported changes in energy demand, exchanger mass, and total annual cost are the direct results of HEN synthesis, not arbitrary manual adjustments.

Data constraints and modelling assumptions

The study is intentionally based on secondary industrial data and literature-derived process models because consistent plantwide primary retrofit data are rarely available across multiple industries. This constraint affects the scope of the analysis in three ways. First, only those midpoint categories for which characterization factors and sufficiently documented inventory flows were available were reported. Second, equipment manufacturing was represented through exchanger-manufacturing mass correlations instead of equipment-specific bills of materials. Third, the environmental inventory excludes plant-specific maintenance frequencies, fouling-cleaning cycles, transportation logistics, and decommissioning because harmonized data for these elements were unavailable across all three cases. These limitations do not invalidate the comparison; however, they should be recognized as constraints on external generalization.

The principal modelling assumptions used throughout the manuscript are summarized here for transparency. (a) The assessment boundary is cradle-to-gate and includes utility generation plus heat-exchanger manufacture, but excludes raw-material extraction differences, product use, and end-of-life because these were assumed unchanged between baseline and retrofit cases. (b) Steam utilities were represented using natural-gas-fired boiler production with 80% thermal efficiency when generated externally; internally generated steam and cooling media were assigned only the electricity burden associated with pumping or fanning. (c) Refrigeration was modelled with R-134a and an annual leak rate of 0.1% of circulating flowrate [20]. (d) Heat-exchanger manufacturing impacts were estimated from exchanger-manufacturing mass predicted from area and number of shells using the vendor-derived correlation shown in Figure 3. (e) All case comparisons used the same functional unit and the same LCIA method so that only process integration effects, not accounting-method changes, drive the comparison. (f) When very-high-temperature process streams were identified by pinch analysis, the results were interpreted as targeting information for staged or specialized recovery devices rather than as an assertion that a single conventional shell-and-tube exchanger can operate across the entire temperature range.

The environmental impacts of heat-exchanger manufacture are commonly reported per kilogram of equipment produced [22]. Aspen Energy Analyzer reports exchanger duties, areas, and network structure, but it does not directly report the fabrication mass of each required unit. Accordingly, exchanger-manufacturing mass was estimated by compiling heat-transfer surface area and mass data from 68 industrial shell-and-tube heat-exchanger models sourced from vendor catalogues. A power correlation between weight and heat-transfer surface area, shown in Figure 3, was then used together with the number of shells to estimate the total exchanger-manufacturing mass required by each HEN. In the results tables, the item previously labeled simply as 'Heat Exchangers [kg]' is therefore more precisely interpreted as 'Estimated exchanger-manufacturing mass [kg]' and is used only as an LCA inventory proxy, not as a direct mechanical design specification. The mass correlation is expressed in eq. (1):

$$W(A,n) = 4.4628A^{1.3007}n^{-0.3007} \quad (1)$$

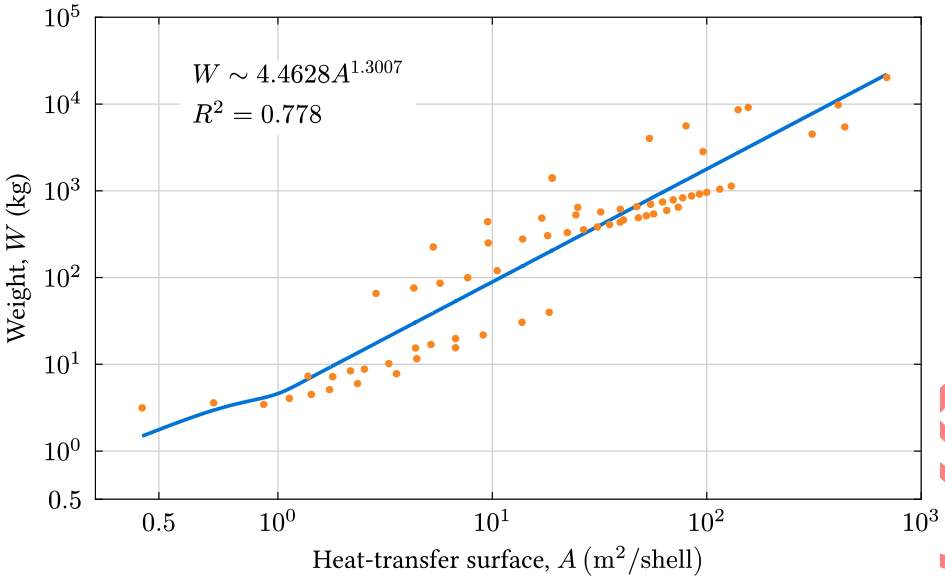

Figure 3. Heat-exchanger weight plotted against heat-transfer surface area of 68 industrial shell-and-tube heat-exchanger models sourced from Ayvaz, AMETEK, and Hexonic. A power function is fitted to the data set with a coefficient of determination of 0.778.

Life cycle impact assessment

Life cycle impact assessment was performed using ReCiPe 2016 at midpoint and endpoint levels [23]. In the present integrated framework, LCA is not an independent parallel exercise. Rather, the post-pinch utility targets and exchanger requirements become the inventory flows that are multiplied by characterization factors. This means that stand-alone PA answers the question 'how much energy and utility demand can be reduced?', stand-alone LCA answers the question 'what is the environmental profile of a given inventory?', and the integrated TPA-LCA framework answers the additional question 'does the environmental benefit of the retrofit remain favourable after the material burden of the retrofit itself is counted?'

Value added by integrating thermal pinch analysis and life cycle assessment

To avoid overstating the conclusions, the results were interpreted at three levels. First, thermal pinch analysis alone was used to report HRAT, total energy reduction, total annual cost change, and the main structural features of the network such as stream splitting, loops, and residual utility placement. Second, LCA of the baseline and retrofitted inventories was used to measure midpoint and endpoint impacts. Third, the integrated interpretation compared these two levels to determine whether the energy benefit of the retrofit remains dominant after exchanger manufacture is included. The contribution of the integration is therefore methodological: PA identifies the retrofit, while LCA tests whether the retrofit is environmentally robust. The midpoint impact calculation used in this transfer is expressed in eq. (1):

$$\mathrm{EI}_j^{\mathrm{mid}} = \sum_j \mathrm{CF}_{i,j}^{\mathrm{mid}} \cdot Q_i \qquad (2)$$

The midpoint values were then translated into their corresponding endpoint environmental impacts, i.e. Damage to Human Health (HH), Damage to Ecosystems (ED), and Damage to Resource Availability (RA), using the characterization factors at endpoint level [23]. Respectively, the endpoint levels are measured in Disability-Adjusted Life Years (DALY), Species-year, and United States dollars (USD2013). DALY represents the number of years lost to premature death or the number of years lived with disability; Species-year represents species

loss integrated over time; and USD2013 represents the additional future extraction costs associated with mineral and fossil resources. The conversion of midpoint to endpoint impacts is represented in eq. (3), where the endpoint impact for category k is obtained from the corresponding midpoint impact and midpoint-to-endpoint characterization factor:

$$\mathrm{EI}_n^{\mathrm{end}} = \mathrm{CF}_{j,n}^{\mathrm{end}} \cdot \mathrm{EI}_j^{\mathrm{mid}} \quad (3)$$

ReCiPe 2016 provides three perspectives used to derive characterization factors: individualist, hierarchist, and egalitarian [23]. The hierarchist perspective was selected in this study because it reflects a balanced and moderate time horizon and considers substances for which there is broad scientific agreement on environmental effects. The characterization factors compiled in Table 1 draw on several source categories. ReCiPe 2016 provides general midpoint and endpoint factors [23]. Wang et al. provided carbon emission inventory data for refrigerant production and recycling [24]. Baral et al. reported upstream climate impact data for mobile air-conditioning refrigerants [25]. Zhang et al. reported life cycle and economic data for hydrofluorocarbon-134a production routes [26]. Batuecas et al. provided life cycle data for heat-transfer fluids [27]. Gaete-Morales et al. supplied fossil-fuel electricity impact factors [28]. Boix Rodríguez et al. supplied heat-exchanger eco-design factors [22]. Table 2 provides the midpoint-to-endpoint characterization factors used to calculate endpoint impacts under the same LCIA perspective.

Table 1. Midpoint characterization factors associated with the life cycle inventory.

Inventory	CF	Unit	Sourced From
R-134a Emission	1549	kg CO_2-eq/kg	ReCiPe 2016
R-134a Production	15.9	kg CO_2-eq/kg	Wang et al. [24]
	2.18×10^{-4}	kg NO_x-eq/kg	Baral et al. [25]
	1.40×10^{-2}	kg Oil-eq/kg	Zhang et al. [26]
Natural Gas (NG) Combustion	5.03×10^{-5}	kg CO_2-eq/kJ	USEPA
	2.11×10^{-9}	kg NO_x-eq/kJ	~100 ppm NO_x flue gas
	2.35×10^{-5}	kg Oil-eq/kJ	ReCiPe 2016
Outsourced Steam	6.29×10^{-5}	kg CO_2-eq/kJ	USEPA
	2.63×10^{-9}	kg NO_x-eq/kJ	From NG boiler operating at 80% thermal efficiency
	2.94×10^{-5}	kg Oil-eq/kJ	
Electricity, Grid	0.4775	kg CO_2-eq/kWh	IEA
	5.64×10^{-5}	kg NO_x-eq/kWh	UNECE
	0.234	kg Oil-eq/kWh	Gaete-Morales et al. [28]
Hitec® molten salt	2.91415	kg CO_2-eq/kg	Batuecas et al. [27]
	2.75×10^{-7}	kg CFC-11-eq/kg	
	5.22×10^{-4}	kg NO_x-eq/kg	
Heat-Exchanger Manufacturing	17.4	kg CO_2-eq/kg	Boix Rodríguez et al. [22]
	9.04×10^{-7}	kg CFC-11-eq/kg	
	8.03×10^{-2}	kg NO_x-eq/kg	
	0.4129	kg Cu-eq/kg	
	4.88	kg Oil-eq/kg	

Table 2. Midpoint-to-endpoint characterization factors provided by ReCiPe 2016.

Endpoint Impact Category	Midpoint to Endpoint CF	Unit
Damage to Human Health	9.28×10^{-7}	DALY/kg CO_2-eq
	5.31×10^{-4}	DALY/kg CFC-11-eq
	9.10×10^{-7}	DALY/kg NO_x-eq
	2.22×10^{-6}	DALY/m^3 H_2O
Damage to Terrestrial Ecosystems	2.80×10^{-9}	Species-year/kg CO_2-eq
	1.29×10^{-7}	Species-year/kg NO_x-eq
	1.35×10^{-8}	Species-year/m^3 H_2O
Damage to Aquatic Ecosystems	7.65×10^{-14}	Species-year/kg CO_2-eq
	1.74×10^{-12}	Species-year/m^3 H_2O
Damage to Resource Availability	0.23	USD_{2013}/kg Cu-eq
	0.457	USD_{2013}/kg Oil-eq

RESULTS AND DISCUSSION

The results presented in this section demonstrate the application of the integrated thermal pinch analysis–life cycle assessment (TPA–LCA) framework to biomass-based industrial systems, with emphasis on ammonia production. The analysis is structured to compare the baseline configuration, in which all thermal duties are satisfied by external utilities, with the thermally integrated configuration obtained through heat-exchanger-network (HEN) synthesis. This comparison enables a simultaneous evaluation of energy performance, economic implications, and environmental consequences. In particular, the redistribution of thermal duties through process-to-process heat exchange is expected to reduce external utility consumption, while introducing additional exchanger-manufacturing requirements that contribute to the life cycle inventory. The integrated interpretation therefore examines whether the operational benefits associated with reduced fuel and utility demand remain dominant when the embodied environmental burden of retrofit implementation is included. This approach provides a consistent basis for assessing the extent to which thermal integration enhances the overall sustainability of ammonia production from biomass.

Ammonia production from biomass

The flowsheet shown in Figure 4 is based on one of the processes presented in the work of Florez-Orrego et al. [29]. The feed, sugarcane bagasse, is first fed into the gasifier and undergoes syngas treatment to maximize the amount of hydrogen (H2) and remove impurities. The exiting gas stream should have enough nitrogen (N2) in a 1:3 molar ratio with H2 and undergoes multistage compression up to 200 bar before being fed to the ammonia production unit. Finally, condensation of ammonia from the leftover gas requires cooling to -20 °C.

For the ammonia case, thermodynamic properties of conventional gas-phase species were calculated using the Soave-Redlich-Kwong equation of state with Boston-Mathias modification, while the nonconventional biomass and ash fractions were evaluated with HCOALGEN and DCOALIGT. Sugarcane bagasse composition was specified according to Table 3, and 100% of the sulfur content was assumed to be organic sulfur. The baseline model was built so that all heating and cooling duties were satisfied by external utilities before HEN synthesis. This baseline assumption is important because it defines the retrofit reference used later in pinch analysis.

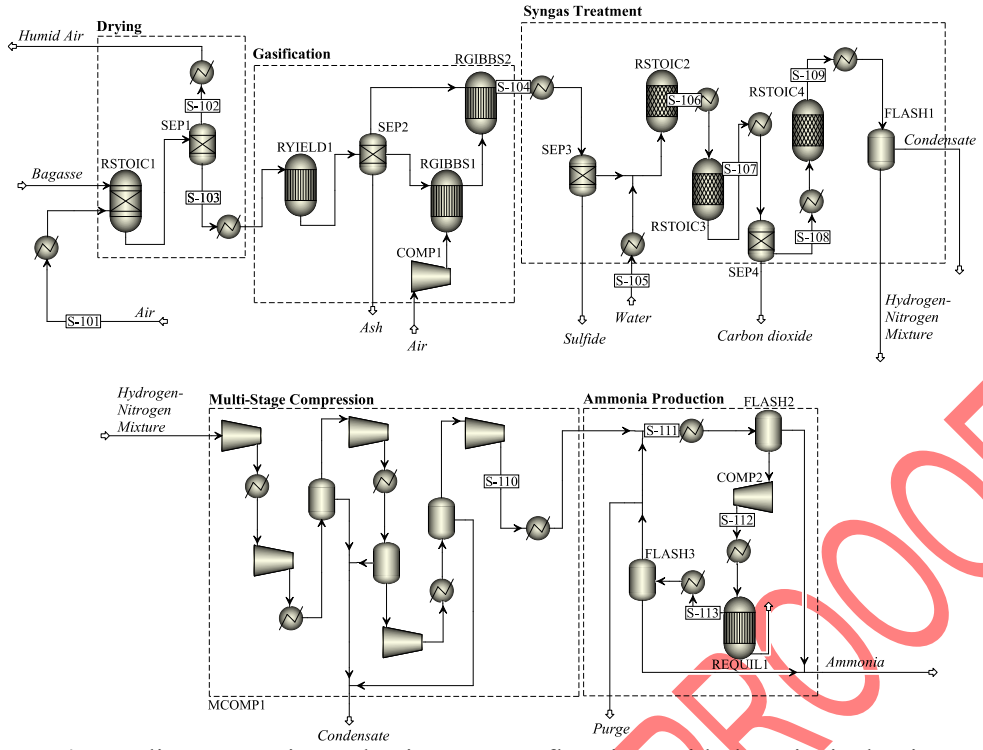

Figure 4. Baseline ammonia production process flowsheet with the principal unit operations identified in the text.

The feed sugarcane bagasse is fed to the drier RSTOIC1 unit where 70% of the moisture content of the biomass is evaporated using hot air at 220 °C. The exiting hot-air stream (S-102) is cooled to 25 °C and the dried biomass stream (S-103) is heated to 700 °C before entering the gasifier. Gasification was modelled by assuming the reactions proceed to equilibrium with no tar modelling. The RYIELD1 unit is where the biomass is decomposed into its elements. Ash, char, and the volatile elements are separated in SEP2, with char to fully combust in RGIBBS1 using air at 1.5 bar. The resulting combustion products and volatile elements from SEP2, are fed to RGIBBS2.

Table 3. Proximate and ultimate analysis of sugarcane bagasse.

Ultimate Analysis [wt% dry basis]						Proximate Analysis [wt% dry basis]			
C	H	N	Cl	S	O	Moisture	Fixed Carbon	Volatile Matter	Ash
50.36	5.644	0.2292	0	0.05730	39.20	14.63	13.69	81.59	4.72

The exiting syngas stream (S-104) is cooled to 400 °C and is fed to a hot gas desulfurization unit (SEP3) and is modelled with a 100% removal of H_2S. The syngas is then reacted with steam in two water gas shift reactors in series (RSTOIC2 and RSTOIC3) where the latter is designed to operate at a lower temperature of 200 °C. The product is then cooled to 120 °C and fed into a CO_2 removal unit modelled at 99.9% efficiency. The RSTOIC4 unit is a methanation unit that removes the leftover CO, and the gas stream is cooled to 30 °C and is flashed before entering the multi-stage compressor unit. The gas stream is mixed with the recycle stream from REQUIL1 and the resulting stream (S-111) is cooled to -20 °C and flashed, where the vapor stream (S-112) is re-compressed to 200 bar and heated to 300 °C before entering the REQUIL1 reactor. The product stream (S-113) is then cooled to 35 °C and flashed.

The optimal HRAT for the ammonia case was 20 °C. At this HRAT, thermal pinch analysis identified a network that transfers heat across multiple temperature intervals, thereby eliminating natural-gas combustion and high-pressure steam purchase while increasing internal

heat recovery. In practical terms, the retrofit requires additional matched process-process exchangers and a reallocation of duties away from utility exchangers. The capital implication is reflected here through the increase in estimated exchanger-manufacturing mass from $1.12E{\times}10^4$ kg to $2.10{\times}10^4$ kg, while the operating implication is reflected through a 76.05% reduction in total energy requirement and a 65.38% reduction in total annual cost. These values constitute the core pinch-analysis results for this case. The resulting network is shown in Figure 5.

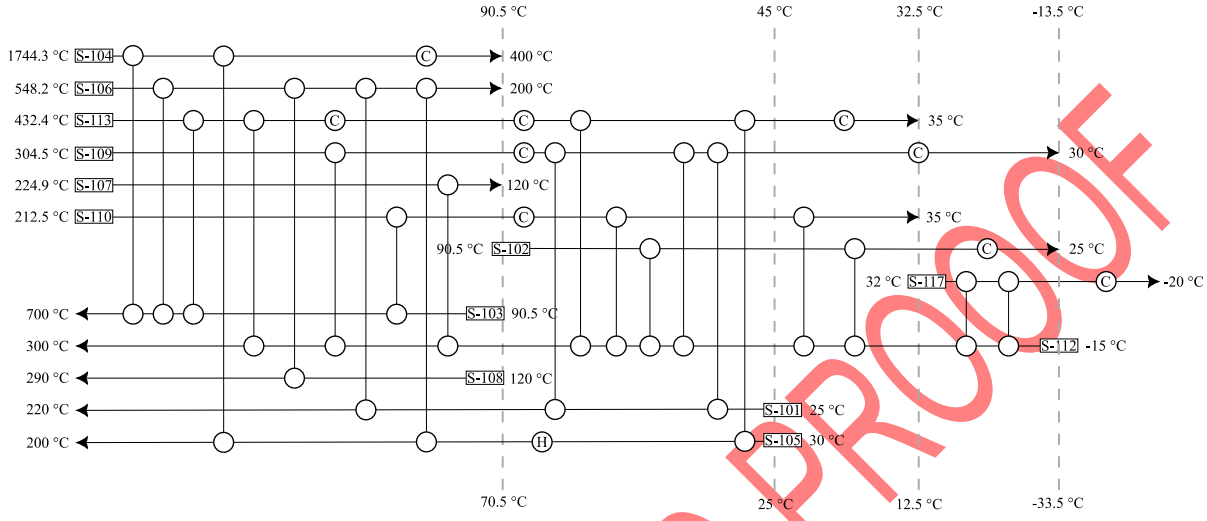

Figure 5. Grid diagram of the HEN of the integrated ammonia process, showing stream temperatures and network topology used for retrofit interpretation.

Particular attention is required for the 1744.3 °C hot stream identified in the grid diagram. This temperature should be interpreted as a process-targeting indicator for the gasification/reforming region rather than as a recommendation for a single conventional exchanger. In practice, heat recovery at this level would be realized through staged cooling, radiant or waste-heat boiler service, refractory-lined syngas coolers, and/or high-temperature alloy or ceramic-contact surfaces before the stream enters conventional convective heat-exchanger service. The HEN insight is therefore thermodynamically meaningful, but the detailed mechanical realization would require high-temperature materials selection and staged exchanger design.

Table 4 summarizes the retrofit-sensitive life cycle inventory flows that changed after HEN synthesis. The baseline design uses utility exchangers for all heating and cooling duties, which explains the initially high natural-gas and steam requirements. After HEN synthesis, external natural-gas combustion, high-pressure steam use, and high-pressure steam generation were eliminated because those duties were met through internal heat recovery. Cooling demand was also reduced for refrigeration and cooling water, although cooling air increased because of the specific utility matches selected by the optimiser. These changes show that the retrofit is not a generic reduction in all utilities; it is a redistribution of duties that follows the thermal structure of the process. The exchanger-related row in Table 4 represents the estimated exchanger-manufacturing mass used as an LCA inventory proxy.

The midpoint environmental impacts are shown in Figure 6a. The integrated process shows substantial reductions in GWI from $2.09{\times}10^5$ to $1.13{\times}10^5$ kg CO_2-eq, POC from 1.96 to 1.08 kg NO_x-eq, WU from 339 to 313 m^3 H2O, and FRD from 411 to 101 kg oil-eq. These improvements are attributed primarily to the lower utility demand of the integrated process. However, there are noticeable increases in SOD from $2.32{\times}10^{-7}$ to $4.33{\times}10^{-7}$ kg CFC-11-eq and MRD from 0.106 to 0.198 kg Cu-eq. These increases arise from the additional exchanger-manufacturing mass required to realize the retrofit, which entails greater use of metals manufacturing processes. The endpoint environmental impacts are shown in Figure 6b. The

integrated process shows consistent and significant reductions across all endpoint categories. HH decreases from 0.194 to 0.105 DALY, ED from 5.89×10^{-4} to 3.20×10^{-4} Species-year, and RA from 188 to 46.4 USD2013. These results indicate that, although the retrofit requires more exchanger material, the reduction in operational utility demand remains dominant in long-term environmental performance.

Table 4. Selected retrofit-sensitive life cycle inventory flows of the baseline and integrated ammonia production process.

Inventory	Baseline Design	Integrated Design
Natural Gas Combustion	7.41×10^{6} kJ/h	0
HP Steam	3.31×10^{6} kJ/h	0
HP Steam Generation	2.47×10^{3} kg/h	0
MP Steam Generation	8.80×10^{2} kg/h	1.26×10^{3} kg/h
Cooling Air	1.03×10^{5} kg/h	3.23×10^{5} kg/h
Cooling Water	3.33×10^{5} kg/h	3.11×10^{5} kg/h
R-134a	8.79×10^{3} kg/h	4.67×10^{3} kg/h
Total Energy Requirement	2.79×10^{7} kJ/h	6.67×10^{6} kJ/h
Estimated Exchanger-Manufacturing Mass	1.12×10^{4} kg	2.10×10^{4} kg

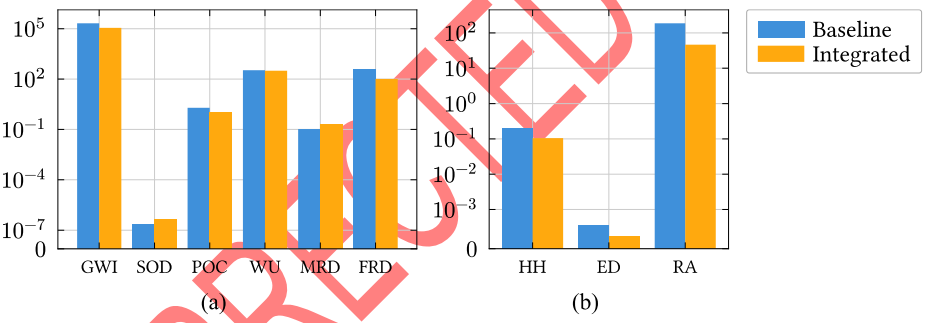

Figure 6. (a) Midpoint and (b) endpoint life cycle impacts of the baseline and integrated ammonia production processes.

Bioethanol production from biomass

The flowsheet shown in Figure 7 is based on the work of Safarian et al. [14]. It starts similarly to the ammonia production process with bagasse as the feedstock. The main advantage of producing bioethanol through this route is that the tar generated within the biomass-conversion train is converted into syngas, whereas conventional bioethanol routes that rely on fermentable sugars commonly treat tar as an undesirable by-product [12]. Fresh syngas is cooled to 37 °C before fermentation, where acetogenic bacteria such as Clostridium ljungdahlii convert the syngas into ethanol and a small amount of acetic acid [13]. Current practice indicates that about 5 wt% ethanol in the broth is near the tolerance limit of the microorganism [13]. The beer is then cooled to remove the spent gas and solid residue before preheating and distillation to near-azeotropic composition. The distillate is then fed to a molecular sieve for final dehydration to fuel-grade ethanol.

For the bioethanol case, the upstream gasification section followed the same nonconventional biomass treatment used for the ammonia case, but phase behavior for conventional components was calculated using Peng-Robinson with Boston-Mathias modification because the process involves gas-liquid equilibrium in fermentation and distillation. The syngas fermentation reactions were modelled in a stoichiometric reactor with

literature-derived fractional conversions, and downstream separation was represented through separators, a distillation column, and a molecular sieve. As in the ammonia case, the baseline model assigned all heating and cooling duties to external utilities before retrofit so that the effect of thermal integration could be isolated.

The fractional conversions for RSTOIC1 were fixed as follows, consistent with syngas-fermentation stoichiometry reported in the literature [30]: 70% of carbon monoxide (CO) forms ethanol, while 5% forms acetic acid, and 50% of H2 forms ethanol, while 2% forms acetic acid. Cooling of the fermenter jacket (S-105) is required to maintain a temperature of 37 °C. The resulting broth then undergoes a series of SEP blocks to separate the solid cake and the spent gas. The resulting beer (S-106) is preheated to 118 °C before entering COL1. All products and by-product streams are cooled to 25 °C, and the resulting ethanol-rich distillate is fed into a molecular sieve (SEP6) that is modelled to recover 99% of the ethanol. The four fermentation reactions are summarised in eqs. (4)-(7):

$$6CO + 3H_2O \rightarrow C_2H_5OH + 4CO_2 \quad (4)$$

$$6H_2 + 3CO_2 \rightarrow C_2H_5OH + 3H_2O \quad (5)$$

$$4CO + 2H_2O \rightarrow CH_3COOH + 2CO_2 \quad (6)$$

$$4H_2 + 2CO_2 \rightarrow CH_3COOH + 2H_2O \quad (7)$$

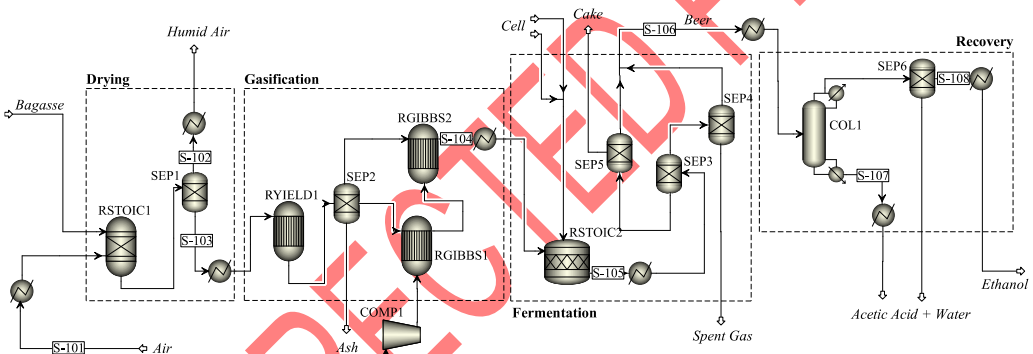

Figure 7. Baseline bioethanol production process flowsheet with the principal unit operations.

The optimal HRAT for the bioethanol case was 5 °C. Thermal pinch analysis showed that the major retrofit opportunity lies in recovering heat around the beer preheating and distillation section, including the interaction between condenser and reboiler duties. The resulting HEN reduces external natural-gas firing almost completely and markedly lowers low-pressure steam, cooling-water, and cooling-air demand. The capital trade-off appears as an increase in estimated exchanger-manufacturing mass from 1.64×10^4 kg to 2.08×10^4 kg, whereas the operating benefit appears as a 62.27% reduction in total energy requirement and a 45.81% reduction in total annual cost. These are the key pinch-analysis outputs that are subsequently carried into the LCA. The network contains multiple loops because the hot streams must be split to satisfy the beer-preheating train, column reboiler demand, and downstream cooling simultaneously. The corresponding grid diagram is shown in Figure 8. In pinch terms, these loops are a consequence of multi-match recovery around the distillation section and do not invalidate the energy target; however, they imply a more demanding control structure and would normally motivate further simplification during detailed retrofit design.

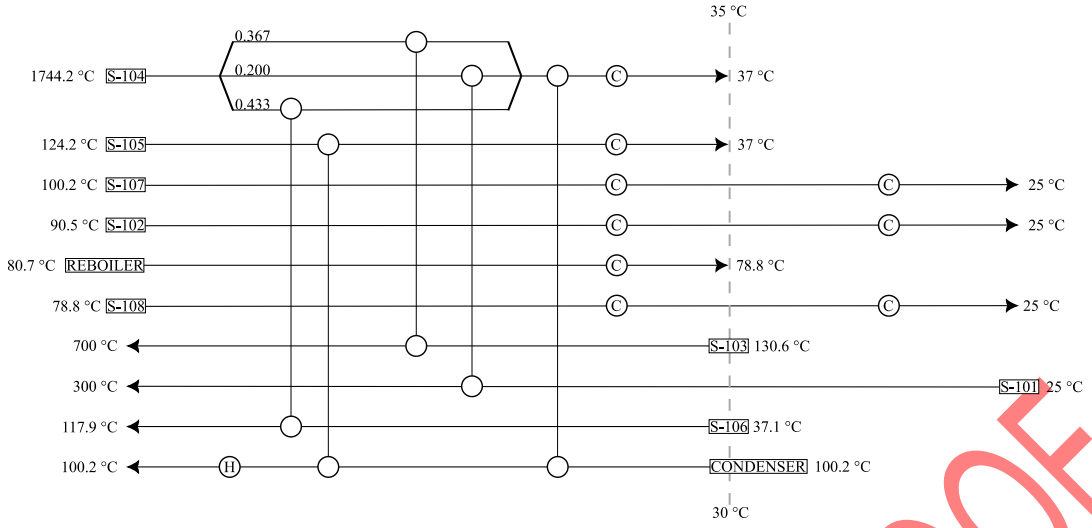

Figure 8. Grid diagram of the HEN of the integrated bioethanol process, showing stream temperatures and the matched-process structure around the distillation section.

Table 5 confirms that the bioethanol retrofit primarily acts by replacing utility duties with internal heat recovery rather than by changing the process chemistry. The baseline representation again uses utility exchangers, so the integrated network can be interpreted as a retrofit that reassigns duties between hot and cold process streams. The very small residual low-pressure steam demand in the integrated case indicates that some duties remain below practical recovery thresholds, which is consistent with pinch constraints. In addition, the apparent use of cold utility below the pinch in the distillation region is attributable to practical separation constraints rather than a violation of pinch rules: the condenser and product-cooling duties are fixed by column temperature levels, product specifications, and finite approach temperatures, while the reboiler requires a stable and controllable heat source. Accordingly, a small amount of residual utility service remains justified even after overall heat recovery has been maximized. The increase in exchanger-manufacturing mass explains why some material-related impacts later rise even as most utility-related impacts decline.

Table 5. Selected retrofit-sensitive life cycle inventory flows of the baseline and integrated bioethanol production process.

Inventory	Baseline Design	Integrated Design
Natural Gas Combustion	2.16×10^{6} kJ/h	0
LP Steam	3.37×10^{6} kJ/h	3.42×10^{2} kJ/h
Cooling Water	3.16×10^{4} kg/h	4.43×10^{3} kg/h
Cooling Air	2.07×10^{6} kg/h	1.16×10^{6} kg/h
Total Energy Requirement	1.67×10^{7} kJ/h	6.28×10^{6} kJ/h
Estimated Exchanger-Manufacturing Mass	1.64×10^{4} kg	2.08×10^{4} kg

The midpoint environmental impacts are shown in Figure 9a. Compared to the baseline, the integrated process shows a reduction in GWI from 668 to 212 kg CO_2-eq, POC from 0.0838 to 0.0616 kg NO_x-eq, WU from 33.2 to 4.6 m^3 H2O, and FRD from 319 to 106 kg Oil-eq. However, there is an increase in SOD from 3.38×10^{-7} to 4.30×10^{-7} kg CFC-11-eq, and MRD from 0.154 to 0.196 kg Cu-eq, which is due to the increased exchanger-manufacturing burden associated with the retrofit. This behavior illustrates the principal value of the integrated framework: although heat integration reduces utility demand and the associated fuel-related impacts, it can simultaneously increase equipment-related burdens. The endpoint results in

Figure 9b show that heat integration still results in overall environmental benefits. HH decreased from 6.94×10^{-4} to 2.07×10^{-4} DALY, ED decreased from 2.33×10^{-6} to 6.64×10^{-7} Species-year, and RA decreased from 146 to 48.4 USD2013. These improvements indicate that operational savings in fuel and utilities have a more significant impact than the environmental contributions associated with the added exchanger hardware.

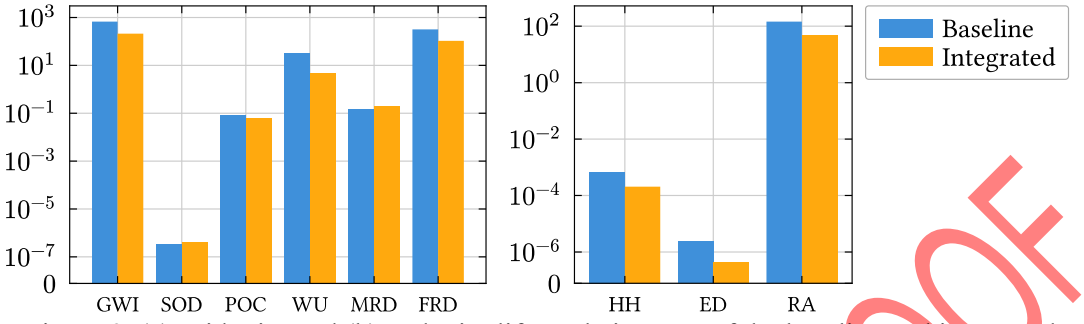

Figure 9. (a) Midpoint and (b) endpoint life cycle impacts of the baseline and integrated bioethanol production processes.

Hydrogen production from biogas

The flowsheet shown in Figure 10 is based on the work of Phan et al. [15]. The production of hydrogen starts with the conversion of purified biogas to syngas by water-gas shift reactors in series. Biogas (S-101) is first compressed to 16 bar and heated to 900 °C before it is fed to a steam reformer (RGIBBS1) alongside steam (S-102) at the same pressure and temperature. Syngas (S-103) is formed and enters the high-temperature shift reactor (RSTOIC1) after cooling to 350 °C, where water and carbon monoxide react to form hydrogen. The product of the exothermic reaction is cooled to 210 °C and then fed to a second water-gas shift reactor (RSTOIC2) operating at a lower temperature. The product (S-105) is cooled to 38 °C and flashed to remove excess water. The dried gas is then fed into a pressure swing adsorber where high-purity hydrogen is collected. The leftover gas from the pressure-swing adsorber, referred to as tail gas, contains unreacted methane, carbon monoxide, and residual hydrogen. The tail gas passes through VALVE1 to relieve the pressure to atmospheric conditions, is mixed with air, and is heated to 250 °C before entering the combustion reactor (RSTOIC3). The energy from the resulting flue gas (S-107) is then recovered.

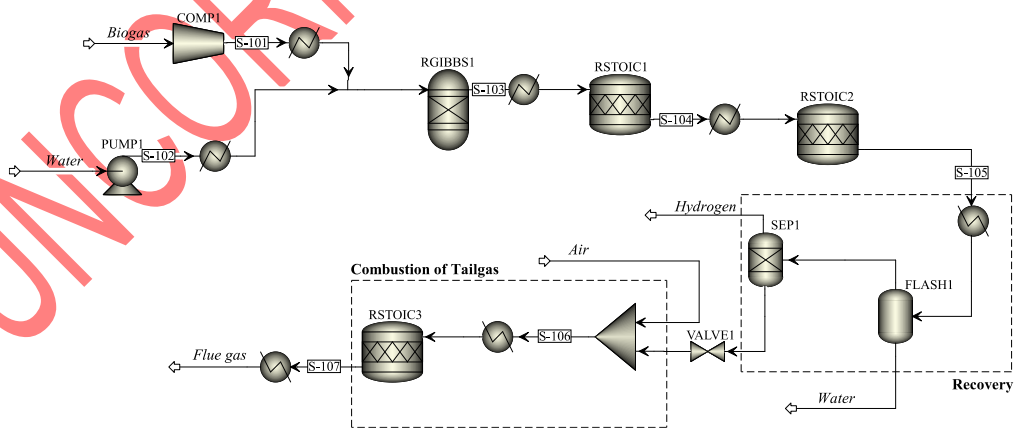

Figure 10. Baseline hydrogen production process flowsheet with the principal unit operations identified in the text.

The optimal HRAT for the hydrogen case was 30 °C. In this process, the retrofit opportunity is governed by the high-temperature reforming and shift sections together with heat recovery from the tail-gas combustion train. The optimised HEN, shown in Figure 11, lowers overall energy requirement by 74.59% and reduces total annual cost by 47.74%. Unlike the ammonia and bioethanol cases, the hydrogen case also decreases the predicted exchanger-manufacturing

mass from 274 kg to 182 kg, indicating that a better duty arrangement can simultaneously improve heat recovery and simplify the required exchanger hardware. This is an important reminder that thermal integration does not necessarily imply higher capital intensity in every case.

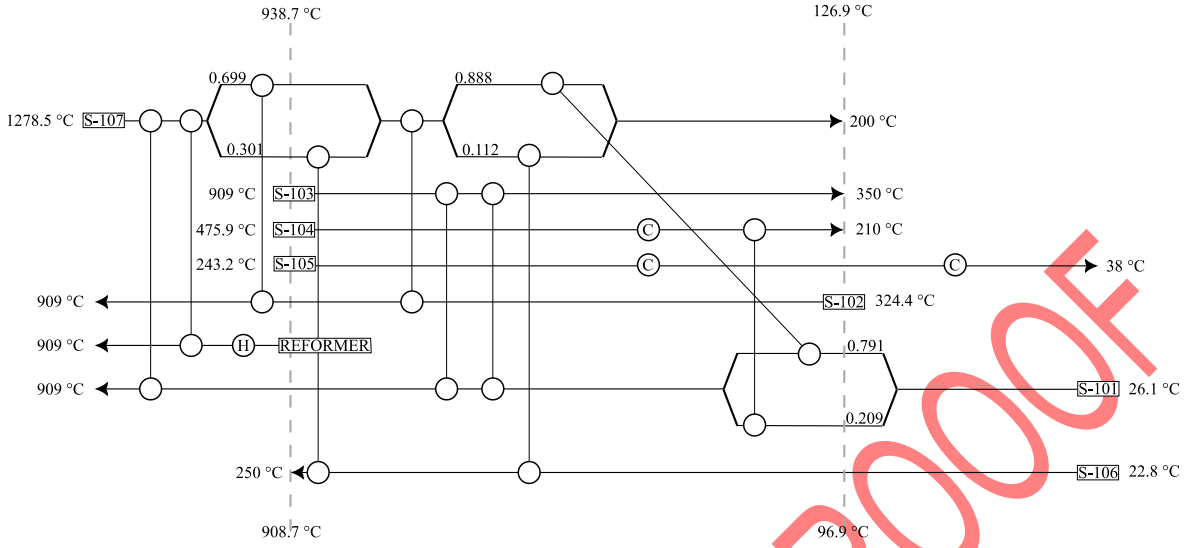

Figure 11. Grid diagram of the HEN of the integrated hydrogen process, showing stream temperatures and network topology after retrofit.

Table 6 shows that the hydrogen retrofit changes the utility portfolio rather than monotonically reducing every single utility. Natural-gas combustion and cooling-water requirement increase for the selected network, while medium-pressure steam generation and hot-oil use are eliminated and high-pressure steam generation is reduced. This pattern demonstrates why energy or carbon conclusions based on a single utility would be incomplete. Only an inventory-based assessment can determine whether the combined effect of all utility changes and exchanger-material changes is favourable. The exchanger-related row in Table 6 again refers to estimated exchanger-manufacturing mass used as an LCA inventory proxy.

Table 6. Selected retrofit-sensitive life cycle inventory flows of the baseline and integrated hydrogen production process.

Inventory	Baseline Design	Integrated Design
Natural Gas Combustion	4.32×10^{5} kJ/h	1.26×10^{6} kJ/h
Cooling Water	3.77×10^{5} kg/h	7.55×10^{3} kg/h
HP Steam Generation	65.5 kg/h	17.7 kg/h
MP Steam Generation	128 kg/h	0
Hot Oil	25.1 kg/h	0
Total Energy Requirement	9.26×10^{5} kJ/h	2.35×10^{5} kJ/h
Estimated Exchanger-Manufacturing Mass	274 kg	182 kg

The comparison between the midpoint environmental impacts can be seen in Figure 12a. There was a significant decrease in GWI from 2470 to 168 kg CO_2-eq, a decrease in SOD from 2.47×10^{-4} to 1.65×10^{-4} kg CFC-11-eq, a decrease in POC from 2.02 to 0.462 kg NO_x-eq, a decrease in MRD from 0.0670 to 0.0447 kg Cu-eq, and a decrease in FRD from 283 to 80.8 kg Oil-eq. However, water usage increased from 103 to 197 m^3 H2O. This reflects that, although some local utility demands increase, the net change across the whole utility portfolio remains environmentally favourable. The comparison between the endpoint environmental impacts of

the baseline and integrated hydrogen production processes is shown in Figure 12b. There is a decrease in all categories, HH from 2.52×10^{-3} to 5.93×10^{-4} DALY, ED from 8.56×10^{-6} to 3.19×10^{-6} Species-year, and RA from 129 to 36.9 USD2013. This further strengthens the argument that a properly targeted HEN retrofit can decrease the overall environmental impact of the chemical process.

Integrated interpretation of pinch analysis and life cycle assessment results

Across the three case studies, PA alone provides the retrofit decision variables, namely HRAT, utility reduction, network complexity, and total annual cost. LCA alone then converts those inventory differences into midpoint and endpoint impacts. The integrated reading of both analyses shows that the operational energy savings dominate the material burden of retrofit in all three cases, but the pattern is case-specific. In the ammonia and bioethanol systems, exchanger-manufacturing mass increases and therefore introduces modest penalties in stratospheric ozone depletion and mineral resource depletion. In the hydrogen system, the optimised network lowers both energy demand and exchanger-manufacturing mass, so the environmental benefit is more uniformly favourable. Without the integrated workflow, these distinctions would not be visible. Equally important, the case studies show that practical retrofit interpretation matters: multiple loops in the bioethanol network signal added control complexity, residual utility around the distillation section remains justified by separation constraints, and the very-high-temperature ammonia stream requires staged or specialized recovery hardware rather than direct conventional exchange, as illustrated in Figure 12.

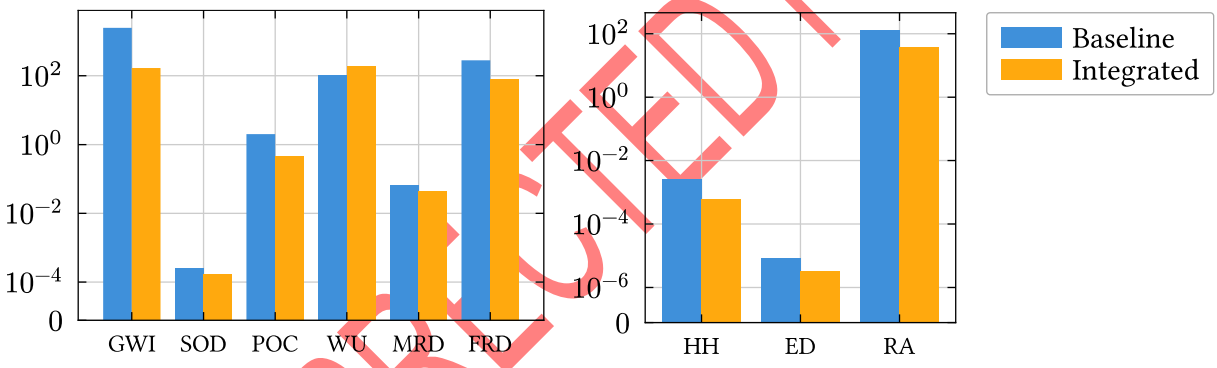

Figure 12. (a) Midpoint and (b) endpoint life cycle impacts of the baseline and integrated hydrogen production processes.

CONCLUSIONS

The two research hypotheses are supported by the results. First, thermal integration substantially reduced external utility demand in all three case studies, with total energy reductions of 62.27–76.05% and total annual cost reductions of 45.81–65.38%. Second, when the retrofit outputs were propagated into the environmental inventory, the integrated thermal pinch analysis–life cycle assessment framework showed that operational savings in fuel and utilities remained dominant over the embodied burden of additional heat-exchanger manufacture. The framework therefore shows clear promise as a screening-level decarbonization tool for energy-intensive industrial systems.

The broader significance of the study is that thermal pinch analysis and life cycle assessment should not be treated as separate reporting tools. For industrial decarbonization, pinch analysis identifies where energy can be recovered, whereas life cycle assessment determines whether that recovery remains environmentally favourable after material embodiment and burden shifting are considered. Across the three case studies, the combined interpretation showed that the environmental outcome of thermal retrofits is case-specific: in the ammonia and bioethanol systems, the added exchanger-manufacturing mass created modest

penalties in stratospheric ozone depletion and mineral resource depletion, while in the hydrogen system the optimised network improved both energy demand and exchanger-material burden. Without the integrated workflow, these distinctions would not have been visible.

From an industrial viewpoint, the proposed framework is economically and environmentally promising, but it should still be applied with engineering judgment. The present results indicate that the decarbonization benefit is robust at screening level; however, project-level decisions should also consider site-specific utility prices, detailed exchanger fabrication data, maintenance and fouling effects, regional electricity mixes, and retrofit constraints imposed by layout and operability. Future work should therefore extend the framework toward uncertainty analysis, plant-specific capital-cost estimation, and multi-objective optimisation that explicitly balances energy, cost, and life cycle impacts.

ACKNOWLEDGMENT(S)

The authors would like to acknowledge Mapúa Malayan Colleges Laguna and Mapúa University for providing institutional support and simulation resources essential to this research.

NOMENCLATURE

Symbols

W	heat exchanger weight	[kg]
A	heat exchanger area per shell	[m^2/shell]
n	number of shells	
Q_i	amount of emission	
EI_j^{mid}	midpoint environmental impact	
$CF_{i,j}^{mid}$	inventory to midpoint factor	
EI_n^{end}	endpoint environmental impact	
$CF_{j,n}^{end}$	midpoint to endpoint factor	

Subscripts and superscripts

i	identity of emission
j	midpoint impact category
n	endpoint impact category

Abbreviations

GHG	Greenhouse Gas
CO_2-eq	Carbon Dioxide-Equivalents
HEN	Heat Exchanger Networks
TAC	Total Annual Cost
MINLP	Mixed Integer Nonlinear Programming
LCA	Life Cycle Assessment
GWP	Global Warming Potential
GWI	Global Warming Impact
LCIA	Life Cycle Impact Assessment
LCI	Life Cycle Inventory
SOD	Stratospheric Ozone Depletion
POC	Photochemical Ozone Creation
WU	Water Usage
MRD	Mineral Resource Depletion

FRD	Fossil Resource Depletion
AEA	Aspen Energy Analyzer
HRAT	Heat Recovery Approach Temperature
HP	High Pressure
MP	Medium Pressure
LP	Low Pressure
CF	Characterization Factors
HH	Damage to Human Health
ED	Damage to Ecosystems
RA	Damage to Resource Availability

REFERENCES

1. Intergovernmental Panel On Climate Change (Ipcc), Ed., "Industry," in *Climate Change 2022 - Mitigation of Climate Change*, 1st ed., Cambridge University Press, 2023, pp. 1161–1244.
2. F. Martins, C. Felgueiras, M. Smitkova, and N. Caetano, "Analysis of Fossil Fuel Energy Consumption and Environmental Impacts in European Countries," *Energies*, vol. 12, no. 6, p. 964, Mar. 2019, https://doi.org/10.3390/en12060964.
3. K. Javan, A. Altaee, S. BaniHashemi, M. Darestani, J. Zhou, and G. Pignatta, "A review of interconnected challenges in the water–energy–food nexus: Urban pollution perspective towards sustainable development," *Sci. Total Environ.*, vol. 912, p. 169319, Feb. 2024, https://doi.org/10.1016/j.scitotenv.2023.169319.
4. P. Comendador, L. Santamaria, M. Amutio, J. Alvarez, M. Olazar, and G. Lopez, "Energy Analysis and Heat Integration in the Joint Process of Biomass Fast Pyrolysis and In Line Sorption Enhanced Steam Reforming," *Energy Fuels*, vol. 38, no. 15, pp. 14402–14413, Aug. 2024, https://doi.org/10.1021/acs.energyfuels.4c02555.
5. F. Wang, L. Wang, A. M. Sadeq, T. R. Alsenani, and T. Muhammad, "Biomass gasification combined with a novel heat integration design for sustainable energy supply programs: Comprehensive thermodynamic, environmental, and economic evaluations," *Energy*, vol. 337, p. 138560, Nov. 2025, https://doi.org/10.1016/j.energy.2025.138560.
6. N. S. Alqahtani, T. A. Alrefai, A. M. Almutlaq, S. M. Alzahrani, and A. E. Abasaeed, "Energy Optimization through Heat and Power Integration on a Chlorobenzenes Production Plant," *Processes*, vol. 12, no. 3, p. 569, Mar. 2024, https://doi.org/10.3390/pr12030569.
7. V. H. Corrêa, C. H. Vassoler, C. B. B. Costa, M. A. D. S. S. Ravagnani, and L. V. Pavão, "Optimization of Heat Integration Systems Considering Multiple Utilities, Organic Rankine Cycles, and Rigorous Thermodynamic Property Calculations," *Ind. Eng. Chem. Res.*, vol. 64, no. 34, pp. 16820–16832, Aug. 2025, https://doi.org/10.1021/acs.iecr.5c02120.
8. X. Gu, F. Ji, L. Liu, and J. Du, "Global Energy Integration for Industrial Parks Incorporating Centralized Trigeneration and Interplant HEN," *Ind. Eng. Chem. Res.*, vol. 62, no. 43, pp. 17805–17823, Nov. 2023, https://doi.org/10.1021/acs.iecr.3c01841.
9. S. Lipiäinen, J. Sillman, E. Vakkilainen, R. Soukka, and M. Tuomaala, "Hydrogen transport options for a large industrial user: Analysis on costs, efficiency, and GHG emissions in steel mills," *Sustain. Prod. Consum.*, vol. 44, pp. 1–13, Jan. 2024, https://doi.org/10.1016/j.spc.2023.11.021.
10. M. B. A. Hassan, F. Charruault, B. Rout, F. N. H. Schrama, J. A. M. Kuipers, and Y. Yang, "A Review of Heat Transfer and Numerical Modeling for Scrap Melting in

Steelmaking Converters," *Metals*, vol. 15, no. 8, p. 866, Aug. 2025, https://doi.org/10.3390/met15080866.

11. T. U. K. Nutakki *et al.*, "Thermo-economic-environmental analysis of a sustainable heat integration design for biomass-fueled power plant using integration of CCHP and sweater desalination application," *Desalination*, vol. 577, p. 117404, May 2024, https://doi.org/10.1016/j.desal.2024.117404.
12. S. Pati, S. De, and R. Chowdhury, "Integrated techno-economic, investment risk and life cycle analysis of Indian lignocellulosic biomass valorisation via co-gasification and syngas fermentation," *J. Clean. Prod.*, vol. 423, p. 138744, Oct. 2023, https://doi.org/10.1016/j.jclepro.2023.138744.
13. V. Ahuja, A. K. Bhatt, B. Ravindran, Y.-H. Yang, and S. K. Bhatia, "A Mini-Review on Syngas Fermentation to Bio-Alcohols: Current Status and Challenges," *Sustainability*, vol. 15, no. 4, p. 3765, Feb. 2023, https://doi.org/10.3390/su15043765.
14. S. Safarian, R. Unnthorsson, and C. Richter, "Bioethanol Production via Herbaceous and Agricultural Biomass Gasification Integrated with Syngas Fermentation," *Fermentation*, vol. 7, no. 3, p. 139, July 2021, https://doi.org/10.3390/fermentation7030139.
15. T. S. Phan, D. Pham Minh, F. Espitalier, A. Nzihou, and D. Grouset, "Hydrogen production from biogas: Process optimization using ASPEN Plus®," *Int. J. Hydrog. Energy*, vol. 47, no. 100, pp. 42027–42039, Dec. 2022, https://doi.org/10.1016/j.ijhydene.2022.01.100.
16. J. Kleinekorte *et al.*, "Life Cycle Assessment for the Design of Chemical Processes, Products, and Supply Chains," *Annu. Rev. Chem. Biomol. Eng.*, vol. 11, no. 1, pp. 203–233, June 2020, https://doi.org/10.1146/annurev-chembioeng-011520-075844.
17. A. Bjørn *et al.*, "Review of life-cycle based methods for absolute environmental sustainability assessment and their applications," *Environ. Res. Lett.*, vol. 15, no. 8, p. 083001, Aug. 2020, https://doi.org/10.1088/1748-9326/ab89d7.
18. M. Bogacka *et al.*, "Life Cycle Assessment (LCA) of the Use of Metallurgical Process Gas for Heat and Electricity, Combined with Salt Removal from Discarded Water," *Sustainability*, vol. 14, no. 3, p. 1205, Jan. 2022, https://doi.org/10.3390/su14031205.
19. D. Koch, A. Friedl, and B. Mihalyi, "Influence of different LCIA methods on an exemplary scenario analysis from a process development LCA case study," *Environ. Dev. Sustain.*, vol. 25, no. 7, pp. 6269–6293, July 2023, https://doi.org/10.1007/s10668-022-02302-w.
20. F. Fabris, M. Fabrizio, S. Marinetti, A. Rossetti, and S. Minetto, "Evaluation of the carbon footprint of HFC and natural refrigerant transport refrigeration units from a life-cycle perspective," *Int. J. Refrig.*, vol. 159, pp. 17–27, Mar. 2024, https://doi.org/10.1016/j.ijrefrig.2023.12.018.
21. A. Rashedi and T. Khanam, "Life cycle assessment of most widely adopted solar photovoltaic energy technologies by mid-point and end-point indicators of ReCiPe method," *Environ. Sci. Pollut. Res.*, vol. 27, no. 23, pp. 29075–29090, Aug. 2020, https://doi.org/10.1007/s11356-020-09194-1.
22. N. Boix Rodríguez, M. Rossi, F. Cappelletti, and C. Favi, "Engineering eco-design of heat exchangers in domestic heating systems using life cycle assessment methodology," *Int. J. Interact. Des. Manuf. IJIDeM*, vol. 18, no. 8, pp. 5749–5771, Oct. 2024, https://doi.org/10.1007/s12008-023-01301-z.
23. M. A. J. Huijbregts *et al.*, "ReCiPe2016: a harmonised life cycle impact assessment method at midpoint and endpoint level," *Int. J. Life Cycle Assess.*, vol. 22, no. 2, pp. 138–147, Feb. 2017, https://doi.org/10.1007/s11367-016-1246-y.
24. H. Wang, Y. Wang, H. Mi, J. Zang, and S. Wang, "Analysis of Carbon Emission Energy Inventory from Refrigerant Production and Recycling Carbon Compensation," *Appl. Sci.*, vol. 12, no. 1, p. 1, Dec. 2021, https://doi.org/10.3390/app12010001.

25. A. Baral, R. Minjares, and R. A. Urban, "Upstream climate impacts from production of r-134a and r-1234yf refrigerants used in mobile air conditioning systems," 2013.
26. S. Zhang, G. Li, B. Bai, L. Qiang, X. Ma, and J. Li, "Life cycle assessment and economic analysis of HFC-134a production from natural gas compared with oil-based and coal-based production," *Front. Chem. Sci. Eng.*, vol. 16, no. 12, pp. 1713–1725, Dec. 2022, https://doi.org/10.1007/s11705-022-2210-y.
27. E. Batuecas, C. Mayo, R. Díaz, and F. J. Pérez, "Life Cycle Assessment of heat transfer fluids in parabolic trough concentrating solar power technology," *Sol. Energy Mater. Sol. Cells*, vol. 171, pp. 91–97, Nov. 2017, https://doi.org/10.1016/j.solmat.2017.06.032.
28. C. Gaete-Morales, A. Gallego-Schmid, L. Stamford, and A. Azapagic, "Life cycle environmental impacts of electricity from fossil fuels in Chile over a ten-year period," *J. Clean. Prod.*, vol. 232, pp. 1499–1512, Sept. 2019, https://doi.org/10.1016/j.jclepro.2019.05.374.
29. A. Flórez-Orrego, R. Nogueira Nakashima, M. E. G. R. Domingos, M. T. Dos Santos, and S. De Oliveira Junior, "Ammonia production from syngas," in *Advances in Synthesis Gas : Methods, Technologies and Applications*, Elsevier, 2023, pp. 45–91.
30. I. Anggraini, M. Tri Ari Penia Kresnowati, R. Purwadi, and T. Setiadi, "Bioethanol Production via Syngas Fermentation," *MATEC Web Conf.*, vol. 156, p. 03025, 2018, https://doi.org/10.1051/matecconf/201815603025.